Effect of electromagnetic parameters on melt flow and heat transfer of AZ80 Mg alloy during differential phase electromagnetic DC casting based on numerical simulation

Yong-hui Jia[1], Cheng-lu Hu[1], *Qi-chi Le[1], and Wen-yi Hu[2]

1. Key Laboratory of Electromagnetic Processing of Materials, Ministry of Education, Northeastern University, Shenyang 110819, China

2. Longyan University, College of Chemistry and Materials Science, Longyan 364012, Fujian, China

Abstract: Based on multi-physical field coupling numerical simulation method, magnetic field distribution, melt flow, and heat transfer behavior of a Φ300 mm AZ80 alloy billet during differential phase electromagnetic DC casting (DP-EMC) with different electromagnetic parameters were studied. The results demonstrate that the increase in current intensity only changes the magnitude but does not change the Lorentz force's distribution characteristics. The maximum value of the Lorentz force increases linearly followed by an increase in current density. As the frequency increases, the Lorentz force's r component remains constant, and the z component decreases slightly. The change in current intensity correlates with the melt oscillation and convection intensity positively, as well as the liquid sump temperature uniformity. It does not mean that the higher the electric current, the better the metallurgical quality of the billet. A lower frequency is beneficial to generate a more significant melt flow rate and velocity fluctuation, which is helpful to create a more uniform temperature field. Appropriate DP-EMC parameters for a Φ300 mm AZ80 Mg alloy are 10–20 Hz frequency and 80–100 A current intensity.

Keywords: heat transfer; melt flow; differential phase electromagnetic field; DC casting; Mg alloy

CLC numbers: TG146.22   **Document code:** A

1 Introduction

Magnesium (Mg) and its alloys are the lightest metal materials, which are as light as plastic and as tough as metal [1]. Therefore, Mg alloys have potential engineering applications in the automotive, military, and aerospace industries, where weight-reduction requirements are continuously increasing to reduce cost or energy consumption [2]. However, magnesium alloys have a limited slip system at low temperatures, which leads to easy cracking during plastic deformation [3]. The metallurgical quality of the deformed billet is closely related to the subsequent deformation behavior. Therefore, obtaining a billet with excellent metallurgical quality is the goal of engineering researchers.

Direct-chill (DC) casting is the primary technology for producing billets of light alloys. The quality of the DC casting billet directly affects the yield, productivity, and properties of the final products. Electromagnetic DC casting is a method that uses melt vibration and convection to obtain grain refinement [4-6]. Many casting technologies have been developed to get excellent solidification structures of billets, based on electromagnetic stirring [7], e.g., casting, refining, and electromagnetic (CREM) process [8], and low-frequency electromagnetic casting (LFEC) [9] process. Some methods are based on electromagnetic vibration, e.g., electromagnetic vibration casting (EVC) [10], and low-frequency electromagnetic vibration casting (LFEVC) [11]. A new process, differential phase electromagnetic casting (DP-EMC) process, was developed based on the above electromagnetic casting processes. The results showed that under the same conditions, the range and magnitude of electromagnetic force in the DP-EMC process became more extensive than those of conventional magnetic fields. The electromagnetic stirring and electromagnetic oscillation can be realized simultaneously [12-14].

*Qi-chi Le

Ph.D, Professor. His research interests mainly focus on casting and solidification, plastic deformation of magnesium alloys, and development of new wrought magnesium alloys. To date, he has published more than 360 peer-reviewed papers and has been granted more than 70 patents.

E-mail: qichil@mail.neu.edu.cn

In electromagnetic DC casting technology, two technologically adjustable parameters, i.e., frequency and current intensity, profoundly affect the solidification structure since the Lorentz force is closely related to heat release and heat removal. The heat removal rate is essential as it determines the casting's solidification time and the temperature distribution in the metals [15]. Bao et al. [16] studied the heat transfer behaviors of AZ80-1%Y alloy during LFEC and found that frequency and excitation current could control the heat transfer behavior by changing the intensity of the forced convection. Le et al. [17] found that lower AC frequency enhanced the penetration depth of the electromagnetic field, and higher AC intensity strengthened vortex agitation. Li et al. [5] produced a magnesium-based AZ61 alloy using an electromagnetic vibration technique and investigated the microstructure development as a vibration frequency function. Jia et al. [18] studied the effects of electromagnetic frequency on solidification characteristics of an AZ80 Mg alloy billet during DC casting. These results show that sufficient refinement of solidification structure can be achieved within a specific frequency range. However, the effect of electromagnetic parameters on melt flow and heat transfer behavior in the liquid sump during differential phase electromagnetic casting (DP-EMC) of Mg alloy billet is still unclear.

The current study aims to comprehensively investigate the effects of the electromagnetic parameters (current intensity and frequency) on characteristics of macro-physical fields during DP-EMC of a Φ300 mm AZ80 Mg alloy billet based on a transient 2D axisymmetric mathematical model that couples the electromagnetic field with fluid flow and solidification. The research results will provide an effective reference for the selecting and adjustment of electromagnetic parameters in the DP-EMC process of magnesium alloy billets.

2 Model description

2.1 Physical model and boundary conditions

Figure 1(a) depicts the electromagnetic DC casting apparatus diagram, mainly consisting of the mold (crystallizer), excitation coils, water cooling system, and melt feeding and control device. During casting, the magnesium melt was poured into the mold through the fluid tube. The water-cooled mold was the primary cooling of the magnesium melt. The resultant round billet was extracted through the dummy bar head. The cooling water ejected from the bottom of the mold through an array of holes produced a series of water jets, which cooled the billet surface as the secondary cooling. The casting was finished when the billet reached the required length.

The geometry model used in the numerical simulation was simplified into a 2D axisymmetric model, as shown in Fig. 1(b). The computational domain comprised a billet with a radius of 150 mm and a length of 400 mm. Previous experiments showed that the assumed length was sufficient to reach a constant temperature profile at the radial direction of the billet bottom. The boundaries were composed of the inlet, free surface, primary cooling, secondary cooling, outlet, and symmetry axis. The heat transfer coefficient boundaries described the separation between the billet and mold during the primary cooling and the contact with water below the mold [19], which were shown in detail in our previous research work [14]. Significantly, in this work, the model was developed to simulate DC casting under the influence of a differential phase electromagnetic field.

2.2 Pulse current waveforms

A schematic diagram of differential phase pulsed voltage and pulse current in a few periods passing through the coils is shown in Fig. 2, where the phase difference is 90°. During the billet's electromagnetic DC casting, the two-phase currents were supplied to two coils, generating a phase difference electromagnetic field in the mold. The current waveforms were measured from electromagnetic field generation and control systems using a digital oscilloscope through the AC/DC clamp. The measured results were fitted mathematically for numerical simulation to obtain the actual electromagnetic field in the crystallizer. The waveforms of the measured differential phase pulse current under different electromagnetic conditions are shown in Fig. 3 [20], including current intensity and
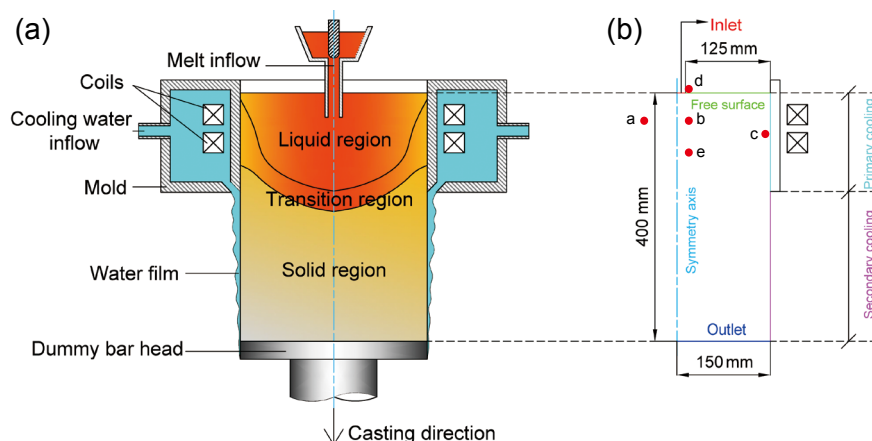

Fig. 1: Schematic diagram of differential phase electromagnetic DC casting (a) and numerical simulation boundaries (b)

electromagnetic frequency. In the electromagnetic DC casting technology, two technologically adjustable parameters, i.e., frequency and electric current intensity, profoundly affect the electromagnetic field's actions. In this work, based on the new differential electromagnetic field, the effects of current intensity and frequency on the melt flow and heat transfer behavior in the liquid sump of the AZ80 alloy DC casting process were studied. The pulse currents (time-average value) were 40 A, 60 A, 80 A, 100 A, and 120 A, respectively, at a constant frequency of 20 Hz. The electromagnetic frequencies were set as 10 Hz, 20 Hz, 25 Hz, 30 Hz, and 40 Hz, respectively, at a constant current of 80 A.

2.3 Description of computational methods

The electromagnetic induction equation was coupled with the fluid flow and heat transfer to calculate the Lorentz force. The distribution of Lorentz force in the molten melt during the electromagnetic DC casting process was obtained by solving Maxwell's equations. The governing equations for momentum and energy transfer during solidification were adapted from Pardeshi et al. [21], with an additional assumption that the solid phase is fixed, resulting in a single-zone model [22]. Lorentz force was added to the momentum equation as a volume force source term. The equivalent specific heat method was used to solve the release of latent heat, assuming that the release of latent heat during solidification was a certain change in the specific heat of the alloy itself. Due to the forced convection in electromagnetic casting, the melt's flow in the mold was in a turbulent state. Therefore, the turbulence was modeled by the standard k-ε model, coupled with the wall function method to describe the viscous flow in the near-wall region simultaneously. The Darcy source was used to simulate the effect of the nature of the mushy region's porosity on the flow field [23], so as to obtain the numerical solution of convection-diffusion-controlled mushy region phase-change problems. The relevant formulas were described and explained in previous studies [14,20] and will not be repeated here. In the simulation, the melt was treated as an incompressible fluid. Calculations of meniscus shape and solute field were not considered.
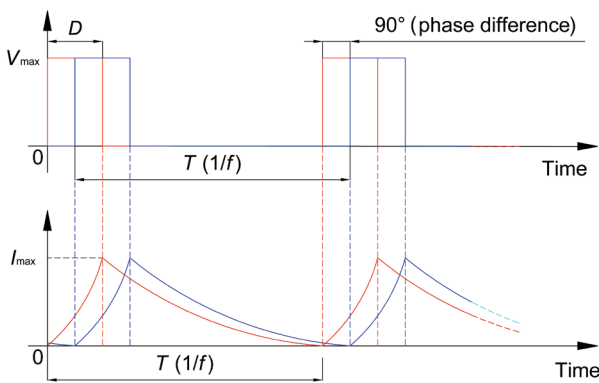

Fig. 2: Schematic diagram of differential phase voltage/current with 90° phase difference

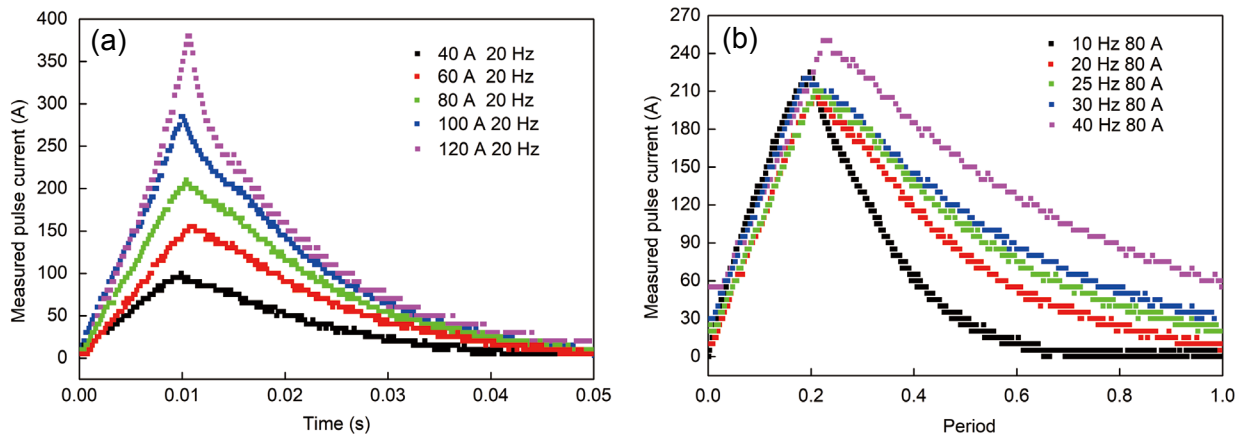Fig. 3: Current waveforms used in the present simulations under different current intensity (a) and frequency (b) [19]

3 Results and discussion

3.1 Magnetic field distribution characteristic of DP-EMC

Figure 4 shows the magnetic field distribution during the electromagnetic DC casting process at a specific moment. The higher magnetic flux density area is mainly concentrated on the primary cooling area [Fig. 4(a)]. Lorentz force's r and z components are shown in Figs. 4(b) and 4(c), respectively. Notably, there are significant differences in the distribution characteristics of Lorentz force along with r and z components. The magnitude of the Lorentz force's r component varies significantly in the radial direction of the mold. The more

significant Lorentz force is mainly distributed at the edge of the liquid sump. The magnitude of the Lorentz force's z component is different in the radial direction and the axial direction. Also, the z-direction components of the Lorentz force on the upper and lower parts of the mold are opposite in direction. The reason is that there is a phase difference between the upper and lower coils, resulting in a spatial difference in intensity and direction of the Lorentz force, which is different from the magnetic field distribution characteristics of conventional electromagnetic DC casting [12,13,24]. This magnitude and distribution of Lorentz force can effectively cause melt oscillation and convection, change melt flow state and temperature distribution, and may be beneficial to refine solidification structure. It will be discussed

in detail in the results of the flow field and temperature field.

Figure 5(a) shows the change of the Lorentz force at Point c [as shown in Fig. 1(b)] in one oscillation period under different current intensities. The Lorentz force shows the same variation trend. The maximum and minimum values of the Lorentz force appear basically at the same time. The increase of current intensity only changes the magnitude but fails to change the Lorentz force's distribution characteristics. With the increase of the current intensity, the Lorentz force increases, and the Lorentz force's maximum value increases linearly, as shown in Fig. 5(b).

Figure 6 shows the variation of Lorentz force with time in an oscillation cycle at different frequencies. As shown in Fig. 6(a), as the frequency increases, the r component of the Lorentz force pointing to the interior of the melt almost does not change, while the peak value pointing to the edge of the melt gradually increases. Besides, according to Fig. 6(b), the increase of frequency gradually decreases the peak value of the z component of Lorentz force from 3,212 N·m^{-3} at 10 Hz to 778 N·m^{-3} at 40 Hz. Therefore, as the frequency increases, the stirring effect of the magnetic field on the melt is also weakened.
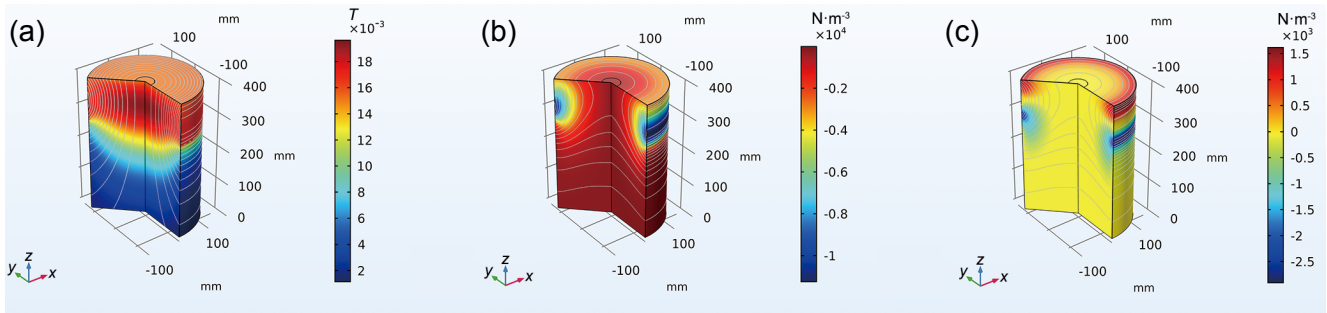

Fig. 4: Magnetic flux density (a), Lorentz force's r component (b), and Lorentz force z component (c) distribution nephogram at representation time during differential phase electromagnetic DC casting
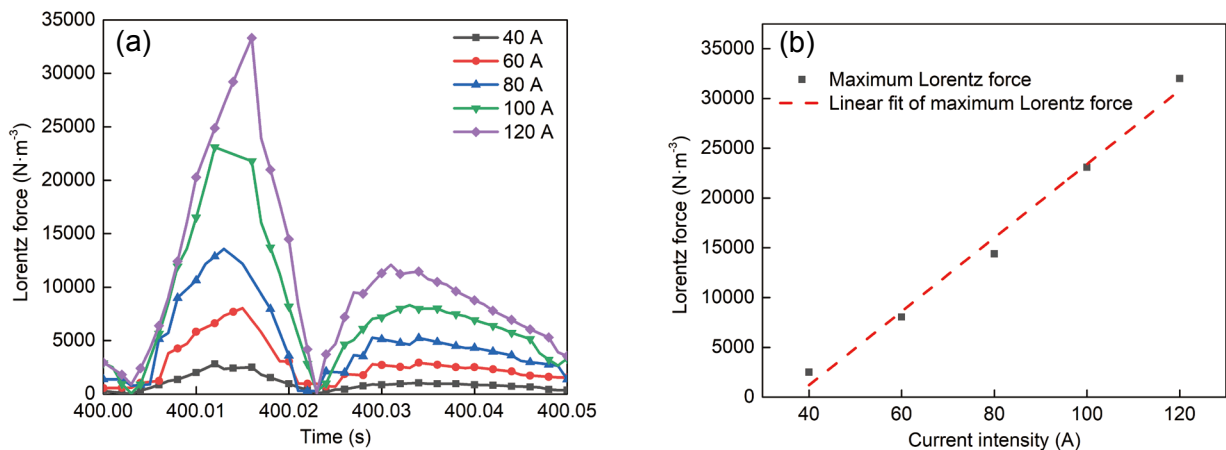

Fig. 5: Variations of Lorentz force in one period (a) and its maximum value (b) with different current intensities
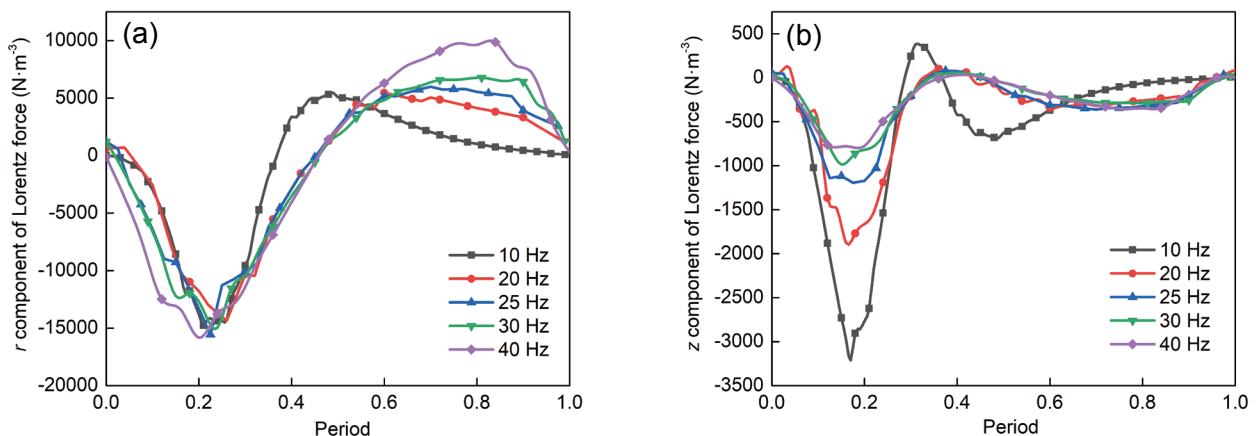

Fig. 6: Lorentz force's r component (a) and z component (b) at Point c within one oscillation period under different frequencies

3.2 Influence of current intensity on macroscopic physical fields

3.2.1 Melt flow

The velocity streamline diagrams of the melt at a specific time in an oscillation period ($\frac{1}{4}T$, $\frac{2}{4}T$, $\frac{3}{4}T$, and $1T$) under different current intensities and a frequency of 20 Hz are shown in Fig. 7, where the gray lines represent the isotherm. During casting, the high-temperature melt flows vertically downward from the gate, forming a clockwise circulation area in the mold. When the current intensity is 40 A, the Lorentz force's disturbance on the melt is weaker, and the maximum flow velocity of the melt is located at the gate. Therefore, the inertial force of the melt entering the liquid sump plays a leading role, which causes the flow to be dominated by natural convection. The central melt's flow velocity is fast, and the flow velocity at the edges is slow. The downward impact of the central high-temperature melt is likely to form a deeper liquid sump. With the increase of the current intensity, the forced convection caused by the electromagnetic field gradually increases. The melt flow velocity in the center of the liquid sump gradually decreases, and the melt velocity on the upper surface and the edge of the liquid sump gradually increases. In addition, under different current intensities, the density of streamline in an electromagnetic oscillation period changes significantly, indicating that the flow velocity of the melt is continually changing under the action of the magnetic field.

The melt at the edge of the liquid sump directly contacts the water-cooled mold, which cools the melt quickly. Its flow velocity and characteristics are critical to the temperature distribution of the entire liquid sump. Nuclei in an experimental casting process are mainly derived from heterogeneous nucleation. The melt velocity near the mold surface is crucial for heterogeneous nucleation [22]. Simultaneously, the melt's flow state at the edge is closely related to the surface quality of the billet. The potential forces can decrease the height of metal in contact with the mold, resulting in modification of the heat flux, which helps to form the progressive decrease in exudation and a smaller segregation zone [8]. The flow state of the melt on the upper surface of the liquid sump is directly related to whether the oxide film formed on the surface of the melt will enter the billet by convection or oscillation of the melt to create oxide inclusions.

To quantitatively analyze the velocity change in the melt, the flow velocities of Point c at the edge of the liquid sump (Fig. 8) and Point d at the upper surface of the liquid sump (Fig. 9) were extracted. With the increase of current intensity, the melt flow velocity at

Point c increases significantly. At a current intensity of 40 A, the maximum melt velocity is 0.0041 m·s⁻¹, which increases to 0.0485 m·s⁻¹ at 120 A. Simultaneously, the magnitude of the melt flow velocity change within an oscillation period also gradually increases. It can be seen from the evolution of the melt flow acceleration at Point c in an oscillation period [Fig. 8(b)] that there are both positive and negative values, and the maximum positive value is greater than the maximum negative value, indicating that the melt is flowing in an oscillatory manner. With the increase of current intensity, the magnitude of acceleration gradually increase. In theory, it is beneficial for the crystal grains to form spherical equiaxed shapes due to forced convection. Based on the "separation theory", the nucleation on the mold wall and the nuclei's detachment are essential in increasing the nucleation
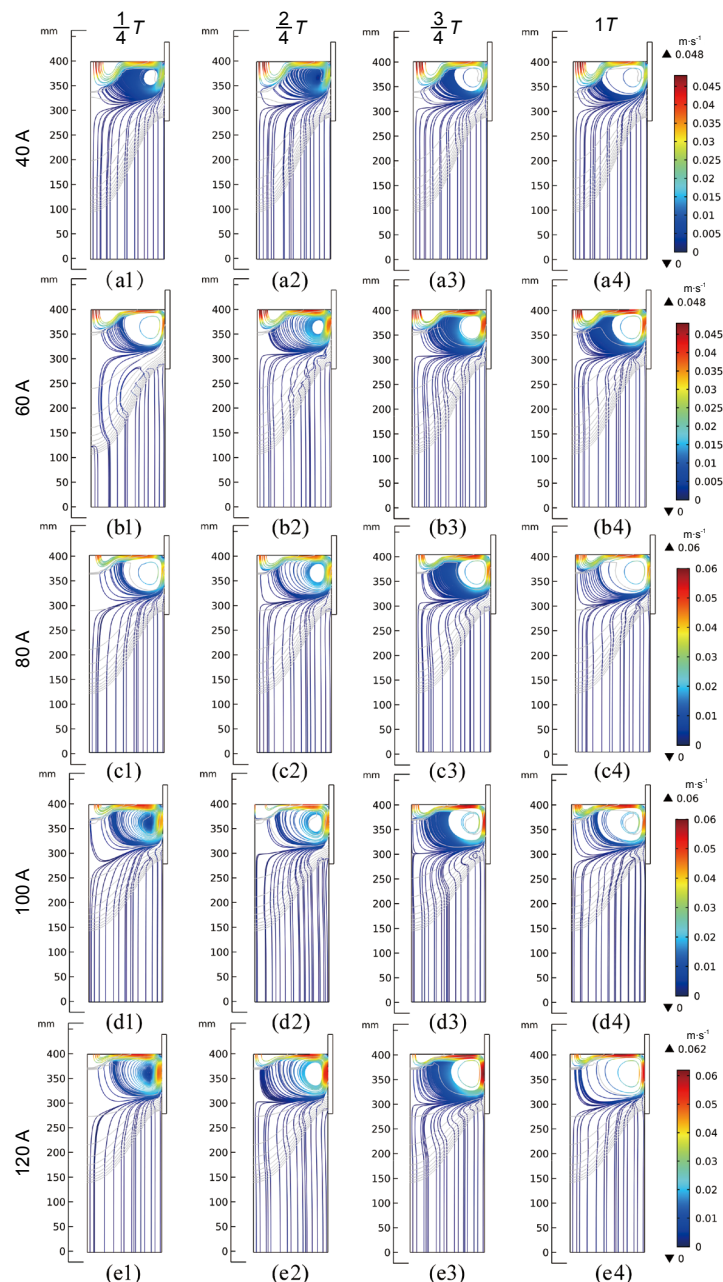

Fig. 7: Velocity streamline diagrams of the melt at a specific time in an oscillation cycle ($\frac{1}{4}T$, $\frac{2}{4}T$, $\frac{3}{4}T$, and $1T$) at a frequency of 20 Hz under 40 A (a1–a4), 60 A (b1–b4), 80 A (c1–c4), 100 A (d1–d4), and 120 A (e1–e4), where the gray lines represent the isotherm

rate [25]. However, with the increase of current intensity, the velocity and amplitude of melt oscillation on the free surface also increase, as shown in Fig. 9. The oxide film formed on the surface is easily destroyed and involved in the solidified structure, causing oxidation inclusions. Therefore, endlessly increasing the current is not helpful to improve the metallurgical quality of the billet. The current intensity should not be too large in the production process. Appropriately increasing the liquid level can solve the secondary inclusions caused by the rupture of the oxide film due to forceful electromagnetic oscillation during the electromagnetic DC casting process.

3.2.2 Heat transfer and solidification

Figure 10 shows the temperature field at a stable stage under different current intensities, mainly showing the temperature gradient in the mushy zone. The blue area is the solid phase zone. It can be seen from the figure that with the increase of the current intensity, the melt temperature in the liquid sump and the depth of the liquid sump are both reduced. The center depth of the liquid sump is 60.5 mm (40 A), 45.4 mm (60 A), 35.9 mm (80 A), 29.7 mm (100 A), and 27.4 mm (120 A), respectively. As already explained in the results of the magnetic field and flow field mentioned above, Lorentz's force puts the
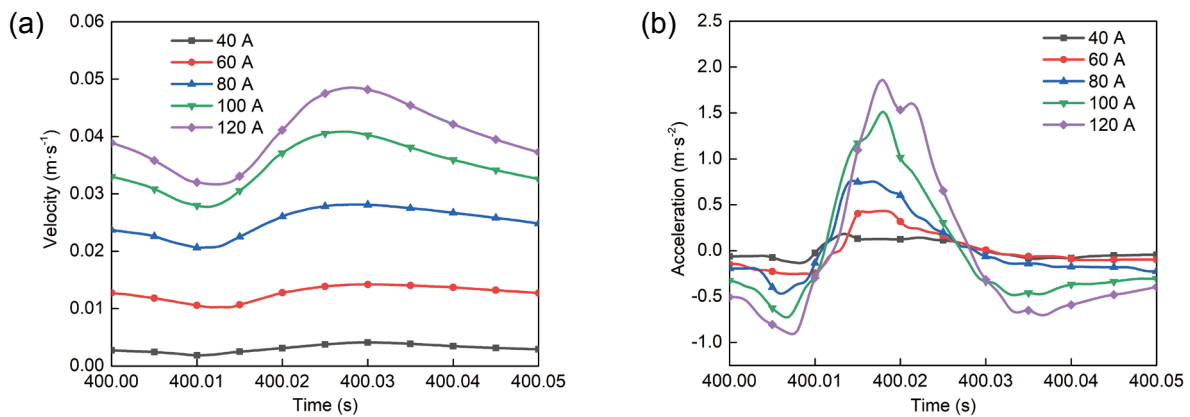

Fig. 8: Variation of velocity (a) and acceleration (b) at edge of liquid sump [Point c in Fig. 1(b)] with time under different current intensities
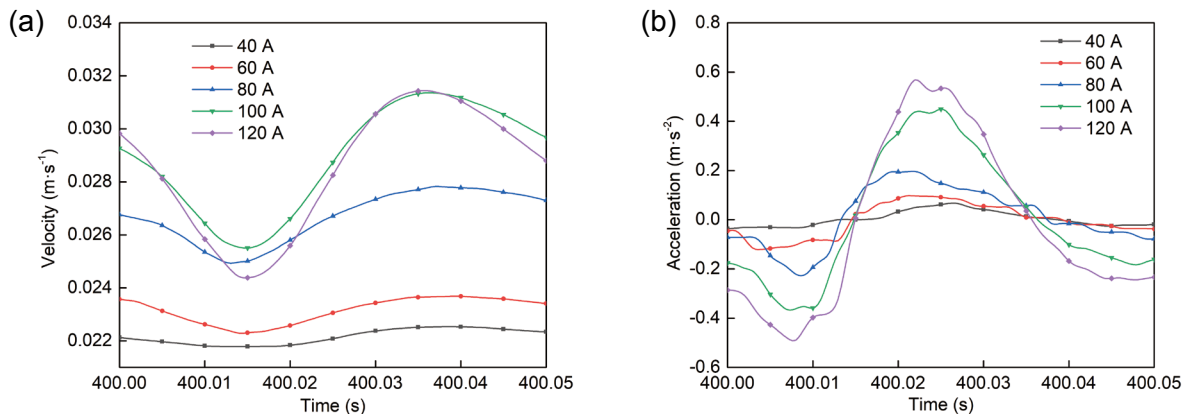

Fig. 9: Variation of velocity (a) and acceleration (b) at upper surface of liquid sump [Point d in Fig. 1(b)] with time under different current intensities
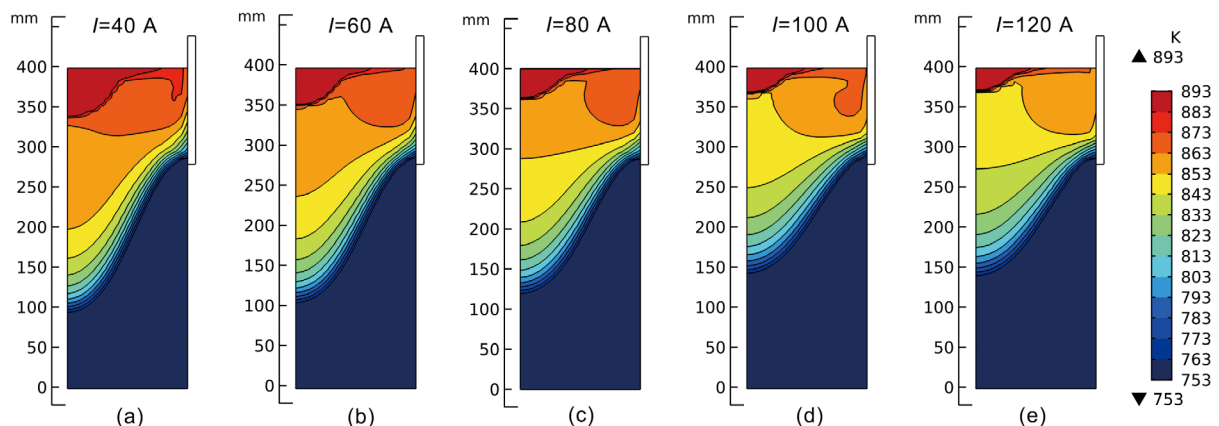

Fig. 10: Temperature gradient in mushy zone at stable stage with 40 A (a), 60 A (b), 80 A (c), 100 A (d), and 120 A (e)

liquid under compression and tension in two successive halves of a cycle. Under these stimulating and vibration effects, the electromagnetic oscillatory wave are transmitted throughout the entire magnesium melt, increasing the heat transport rate of the liquid, which is beneficial for superheat removal [10]. With the increase of current intensity, the escape of superheat is enhanced, and the melt temperature is rapidly homogenized.

The melt temperature changes from the center to the edge [the line in which Points a and c are located, as shown in Fig. 1(b)] of the liquid sump in Fig. 11(a) shows that the temperature in the radial direction of the liquid sump gradually decreases with the increase of the current intensity. When the current intensity is 40 A, the convection and oscillation effects of the melt are weaker. Therefore, it is difficult for the high-temperature melt in the center of the liquid sump to dissipate heat. In contrast, the liquid at the edge of the water-cooled mold dissipates heat faster, eventually leading to a significant radial temperature difference, that is a high-temperature distribution inside and low-temperature distribution outside. As the current intensity increases, the melt oscillation and convection effects increase, the melt flow velocity increases, and the heat dissipation efficiency improves significantly. Therefore, when the current intensity is higher than 40 A, the temperature is low at the center and edge of the liquid sump, and high at 1/2 radius. In particular, it is worth noting that as the current intensity increases, the temperature in the center of the liquid sump gradually decreases while the temperature at the edge slightly increases. The temperature difference between the center and the liquid sump edge is shown in Fig. 11(b). The reasons are as follows: on the one hand, in the steady-state electromagnetic DC casting process, the water-cooled mold wall first cools the melt to form a solidified shell. Afterward, as the solidified shell pulls away from the mold wall due to shrinkage and thermal contraction, the thermal contact between the melt and the mold becomes weaker, resulting in a sudden decrease in heat flux. When the circulation of the melt strengthens with the increase of the current intensity, the high-temperature melt in the center transfers to the edges faster, resulting in higher temperature and faster heat dissipation at the edge of the billet. Simultaneously, due to the circulation, the melt at about 1/4 of the radius from the edge does not flow (as shown in Fig. 7),

which causes the low heat exchange efficiency and the high melt temperature. On the other hand, the radial force of Lorentz force (Lorentz force's r component) can achieve soft contact between the melt and the casting mold, making the heat transfer efficiency at the edge lower. Greater current intensity means a more vigorous melt convection and larger Lorentz force's r component, that is, weaker heat exchange capacity at the edge of billet.

In combination with the above analysis of flow field and temperature field, it can be concluded that at a fixed frequency (20 Hz), for the electromagnetic DC casting of AZ80 magnesium alloy billet with a diameter of 300 mm, the application of 80–100 A oscillating current is more conducive to obtain a fine and uniform solidification structure, which can effectively reduce the possibility of secondary oxidation inclusion.

3.3 Influence of pulse frequency on macroscopic physical fields

3.3.1 Melt flow

In electromagnetic DC casting, the determination of an optimal frequency is difficult, as it affects the magnitude and distribution of Lorentz force in the mold and is closely related to the interaction rate of the magnetic field and melt. Figure 12 shows the velocity streamline diagrams of the melt at a specific time in an oscillation period ($\frac{1}{4}T$, $\frac{2}{4}T$, $\frac{3}{4}T$, $1T$) at different pulse frequencies and a current of 80 A, where the gray lines represent the isotherms. With the increase of frequency, the velocity in the center of the liquid sump increases gradually. In contrast, the melt velocities on the upper surfaces and edge of the liquid sump decrease progressively. The variation trend of melt flow at different frequencies during one oscillation cycle is different with that at different currents. At the frequency of 10 Hz or 20 Hz, the maximum melt flow velocity is concentrated near the melt surface and the mold's inner wall. The velocity decreases with the increase of the frequency. When the frequency increases to 25–40 Hz, the maximum melt flow velocity is concentrated at the gate, which is different from the flow field at the above two frequencies. Therefore, the maximum melt velocity cannot reflect the change of melt velocity caused by frequency change.
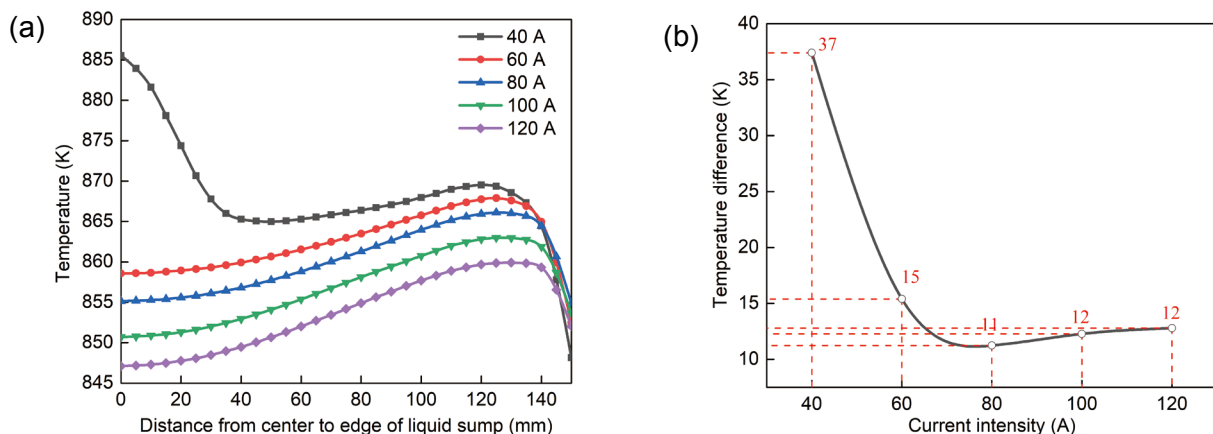
(a)

(b)

Fig. 11: Temperature change from center to edge (the radius from Points a to c) of liquid sump (a) and the maximum temperature difference of the melt in the radial direction (b) under different current intensities

Further analysis of the velocity changes at Point c near the inner wall of the mold at different frequencies shows that the lower the frequency, the greater the melt's velocity, which is consistent with the trend of Lorentz force, as shown in Fig. 13(a). The variation of velocity maximum and fluctuation amplitude with frequency shows that the maximum velocity decreases with the increase of frequency at a lower frequency (less than 30 Hz). When the frequency increases from 10 Hz to 20 Hz, the oscillation amplitude of the velocity decreases. When the frequency further increases, the oscillation amplitude of the velocity remains almost unchanged. However, a minor frequency means that the frequency of convection and oscillation of the melt driven by the magnetic field simultaneously is low. Only from the perspective of melt flow, under a fixed current intensity, the optimum flow pattern can be obtained by applying a lower frequency (less than 20 Hz) of the electromagnetic field, which, in turn, reduces the macrosegregation to the maximum extent.

3.3.2 Heat transfer and solidification

Figure 14 shows the temperature field at the stable stage under different frequencies, mainly showing the temperature gradient in the mushy zone, in which the blue area is the solid phase zone. It can be seen that with the increase of the frequency, the change in melt temperature distribution is not significant, compared to the instability caused by the difference in current intensity. The area of the high-temperature zone and the depth of the liquid sump are slightly increased. The melt temperature variation from the center to the edge [the line in which Points a and c are located, as shown in Fig. 1(b)] of the liquid sump [Fig. 15(a)] shows that the heat exchange between the melt and the water-cooled mold is relatively weak, and the influence of frequency on the melt temperature
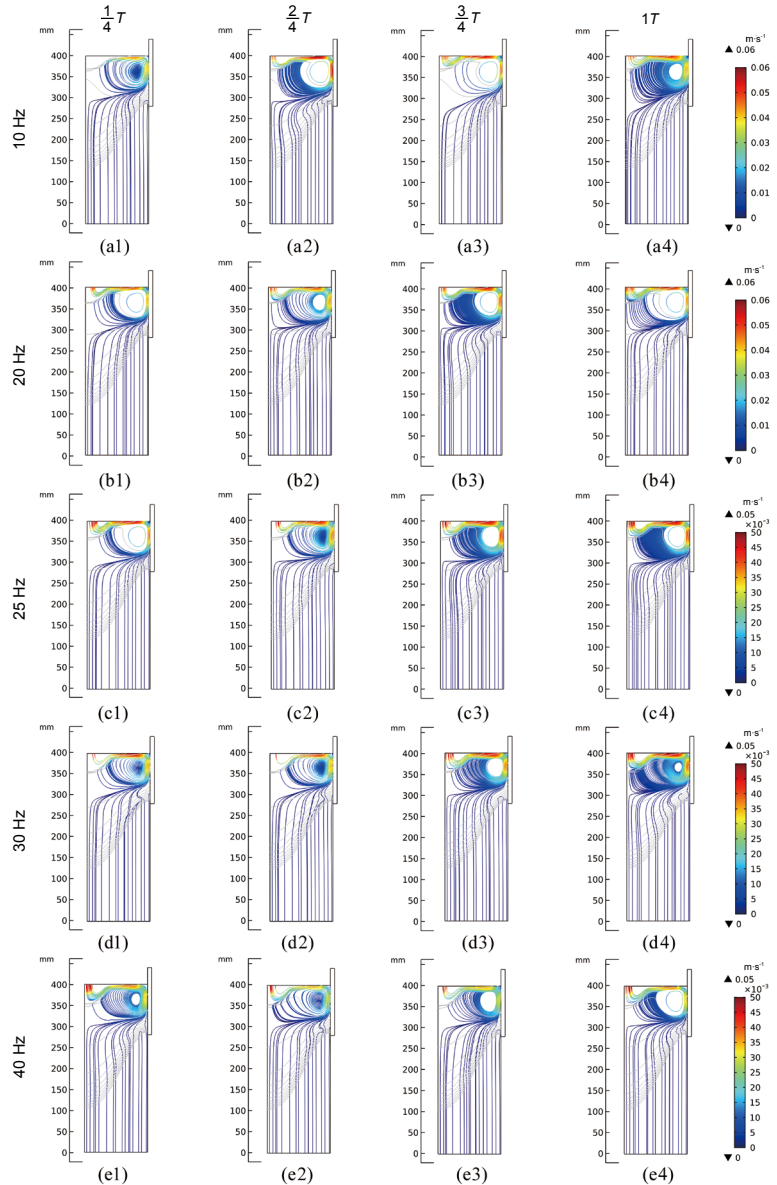

Fig. 12: Velocity streamline diagrams of melt at a specific time in an oscillation period ($\frac{1}{4}T$, $\frac{2}{4}T$, $\frac{3}{4}T$, and $1T$) at a current of 80 A under 10 Hz (a1–a4), 20 Hz (b1–b4), 25 Hz (c1–c4), 30 Hz (d1–d4), and 40 Hz (e1–e4), where the gray lines represent the isotherms
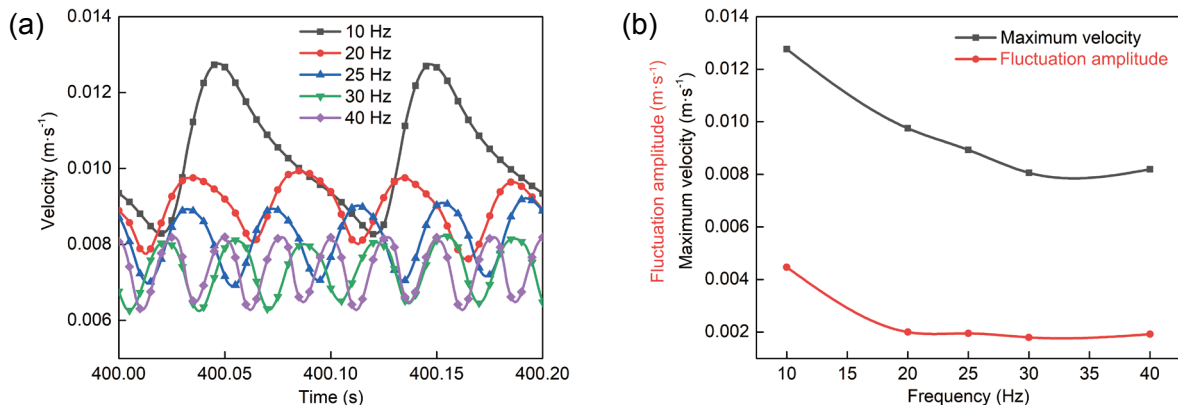

Fig. 13: Variation of velocity (a) and maximum velocity and fluctuation amplitude (b) at Point c under different frequencies
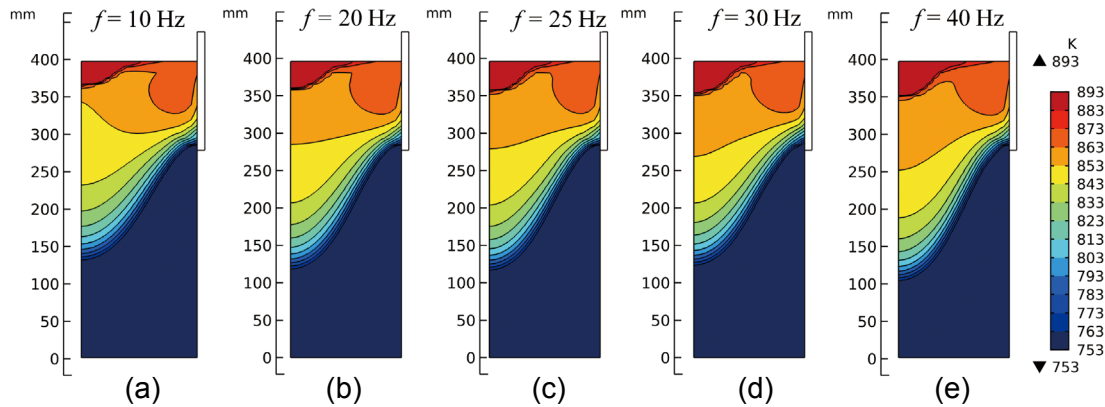
Fig. 14: Temperature gradient in mushy zone at the stable stage under frequencies of 10 Hz (a), 20 Hz (b), 25 Hz (c), 30 Hz (d), and 40 Hz (e)
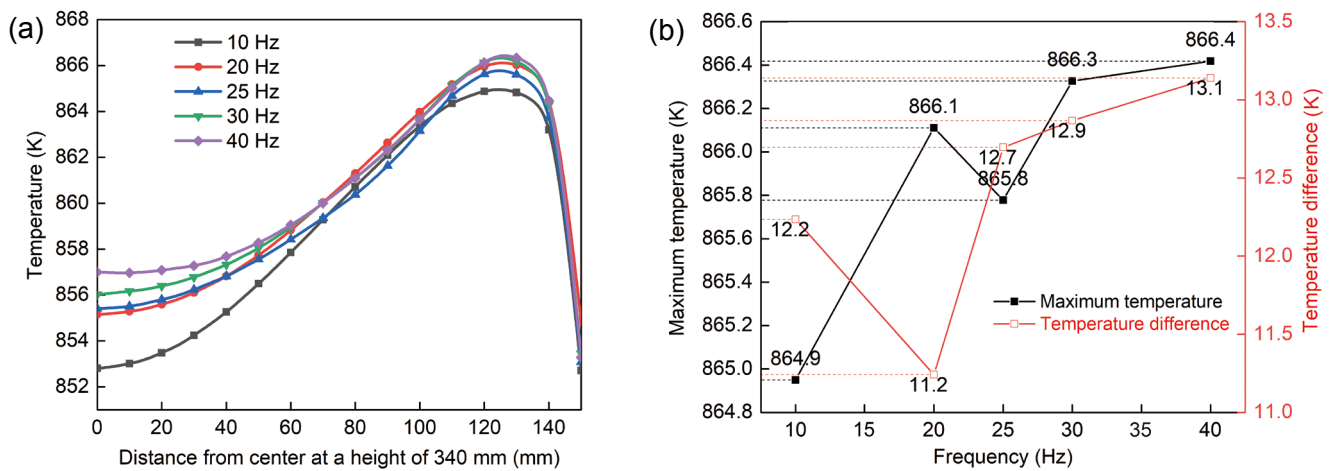

Fig. 15: Changes of temperature from center to edge (the radius from Point a to Point c) of liquid sump (a) and the maximum temperature and temperature difference in the above results (b) under different frequencies

at the edge of the billet is not apparent. At the same time, the temperature of the center melt increases slightly when the frequency increases. After extracting the temperature data of the path as mentioned above and analyzing the melt temperature difference, as shown in Fig. 15(b), it is found that the melt temperature difference is more negligible at lower frequencies (10 Hz and 20 Hz), indicating that the radial temperature distribution of the liquid sump is uniform. In comparing 10 Hz and 20 Hz, the maximum melt temperature is higher at 20 Hz, but the radial temperature difference is smaller, while it is opposite at 10 Hz. This is because at 20 Hz and 10 Hz, the magnitude of the melt velocity and its change frequency are obviously different, and the magneto-induced convection effect at 20 Hz is weaker than that at 10 Hz, so the effect on the high temperature area near the edge is smaller. The weaker magnetic field weakens the interface heat dissipation caused by convection at the wall. The combined effect leads to a higher maximum temperature and a smaller temperature difference at 20 Hz.

The analysis of the flow field and temperature field mentioned above shows that under a fixed current intensity (80 A), for the electromagnetic DC casting of AZ80 magnesium alloy round

billets with a diameter of 300 mm, a lower electromagnetic frequency (10–20 Hz) is more conducive to obtaining a better-solidified structure.

4 Conclusions

In the present study, using the numerical simulation method, the effects of electromagnetic parameters on macro-physic fields in DP-MEC of a Φ300 mm AZ80 Mg alloy billet were studied systematically. The main conclusions are as follows:

(1) As the current intensity increases, the Lorentz force in the melt increases linearly. As the frequency increases, the Lorentz force's r component remains unchanged, and the z component decreases slightly.

(2) The current intensity change is positively correlated with changes in melt flow velocity, velocity oscillation amplitude, cooling rate, and temperature distribution uniformity in the liquid sump.

(3) The frequency has less influence on the temperature field. It is more favorable to generate a higher melt flow rate and more significant velocity fluctuation at a lower frequency, so as to obtain a more uniform temperature field.

(4) For the differential phase electromagnetic casting of Φ300 mm AZ80 magnesium alloy billets, appropriate electromagnetic parameters are: current intensity of 80–100 A and frequency of 10–20 Hz.

Acknowledgements

References

[1] Karanpreet S, Suri N M. Magnesium alloys and its machining: A review. International Research Journal of Engineering and Technology, 2016, 3(5): 9.

[2] Jia W T, Ma L F, Jiao M Y, et al. Fracture criterion for predicting edge-cracking in hot rolling of twin-roll casted AZ31 Mg alloy. Journal of Materials Research and Technology, 2020, 9(3): 4773–4787.

[3] Jia W T, Ma L F, Le Q C, et al. Deformation and fracture behaviors of AZ31B Mg alloy at elevated temperature under uniaxial compression. Journal of Alloys and Compounds, 2019, 783: 863–876.

[4] Guo S J, Le Q C, Zhao Z H, et al. Microstructural refinement of DC cast AZ80 Mg billets by low frequency electromagnetic vibration. Materials Science and Engineering: A, 2005, 404(1–2): 323–329.

[5] Li M, Tamura T, Omura N, et al. The solidification behavior of the AZ61 magnesium alloy during electromagnetic vibration processing. Journal of Alloys and Compounds, 2010, 494(1–2): 116–122.

[6] Guo S J, Le Q C, Han Y, et al. The effect of the electromagnetic vibration on the microstructure, segregation, and mechanical properties of as-cast AZ80 magnesium alloy billet. Metallurgical and Materials Transactions A, 2006, 37(12): 3715–3724.

[7] Mi J, Eskin D G. Solidification processing of metallic alloys under external fields. New York: Springer, 2018.

[8] Vives C. Electromagnetic refining of aluminum alloys by the CREM process: Part I. Working principle and metallurgical results. Metallurgical Transactions B, 1989, 20(5): 623–629.

[9] Zhang B J, Cui J Z, Lu G M. Effects of low-frequency electromagnetic field on microstructures and macrosegregation of continuous casting 7075 aluminum alloy. Materials Science and Engineering: A, 2003, 355(1–2): 325–330.

[10] Vivès C. Effects of forced electromagnetic vibrations during the solidification of aluminum alloys: Part II. Solidification in the presence of colinear variable and stationary magnetic fields. Metallurgical and Materials Transactions B, 1996, 27(3): 457–464.

[11] Dong J, Cui J Z, Ding W J. Theoretical discussion of the effect of a low-frequency electromagnetic vibrating field on the as-cast microstructures of DC Al-Zn-Mg-Cu-Zr ingots. Journal of Crystal Growth, 2006, 295(2): 179–187.

[12] Jia Y H, Chen X R, Le Q C, et al. Numerical study on action of HMF, PMF, DHMF, and DPMF on molten metal during electromagnetic casting. The International Journal of Advanced Manufacturing Technology, 2019, 103(1–4): 201–217.

[13] Jia Y H, Chen X R, Le Q C, et al. Macro-physical field of large diameter magnesium alloy billet electromagnetic direct-chill casting: A comparative study. Journal of Magnesium and Alloys, 2020, 8(3): 716–730.

[14] Wang H, Jia Y H, Le Q C, et al. Transient numerical simulation of solidification characteristic under differential phase pulsed magnetic field. Computational Materials Science, 2020, 172: 109261.

[15] Su X, Feng Z J, Huang J H, et al. Influence of a low-frequency alternating magnetic field on hot tearing susceptibility of EV31 magnesium alloy. China Foundry, 2021, 18(3): 229–238.

[16] Bao L, Zhang Z P, Le Q, et al. Heat transfer behavior of AZ80-1%Y alloy during low-frequency electromagnetic casting. Transactions of Nonferrous Metals Society of China, 2015, 25(11): 3618–3624.

[17] Le Q C, Guo S J, Zhao Z H, et al. Numerical simulation of electromagnetic DC casting of magnesium alloys. Journal of Materials Processing Technology, 2007, 183(2–3): 194–201.

[18] Jia Y H, Le Q C, Liao Q Y, et al. The effect of frequency on solidification characteristics of AZ80 alloy during electromagnetic DC casting. Materials Research Express, 2019, 6(12): 126549.

[19] Hao H, Maijer D M, Wells M A, et al. Development and validation of a thermal model of the direct chill casting of AZ31 magnesium billets. Metallurgical and Materials Transactions A, 2004, 35(12): 3843–3854.

[20] Jia Y H, Wang H, Le Q C. Transient coupling simulation of multi-physical field during pulse electromagnetic direct-chill casting of AZ80 magnesium alloy. International Journal of Heat and Mass Transfer, 2019, 143: 118524.

[21] Pardeshi R, Singh A K, Dutta P. Modeling of solidification process in a rotary electromagnetic stirrer. Numerical Heat Transfer, Part A: Applications, 2008, 55(1): 42–57.

[22] Chen Q, Shen H. Numerical study on solidification characteristics under pulsed magnetic field. International Journal of Heat and Mass Transfer, 2018, 120: 997–1008.

[23] Voller V R, Prakash C. A fixed grid numerical modelling methodology for convection-diffusion mushy region phase-change problems. International Journal of Heat and Mass Transfer, 1987, 30(8): 1709–1719.

[24] Zhang H T, Nagaumi H, Cui J Z. Coupled modeling of electromagnetic field, fluid flow, heat transfer and solidification during low frequency electromagnetic casting of 7XXX aluminum alloys. Materials Science and Engineering: A, 2007, 448(1–2): 177–188.

[25] Ohno A. Solidification – The Separation theory and its practical applications. First edition. Springer-Verlag Berlin Heidelberg, 1987.